Colloidal CdSe/CdS Dot-in-Plate Nanocrystals with 2D-Polarized Emission

Elsa Cassette,[†] Benoît Mahler,[†] Jean-Michel Guigner,[‡] Gilles Patriarche,[§] Benoît Dubertret,[†,*] and Thomas Pons[†,*]

[†]Laboratoire Physique et Etude des Matériaux, ESPCI/CNRS/UPMC UMR 8213, 10, rue Vauquelin, 75005 Paris, France, [‡]Institut de minéralogie et de physique des milieux condensés, CNRS/UPMC/IRD UMR 7590, 4, place Jussieu, 75252 Paris Cedex 05, France, and [§]Laboratoire de Photonique et de Nanostructures, CNRS UPR20, route de Nozay, 91460 Marcoussis, France

ABSTRACT

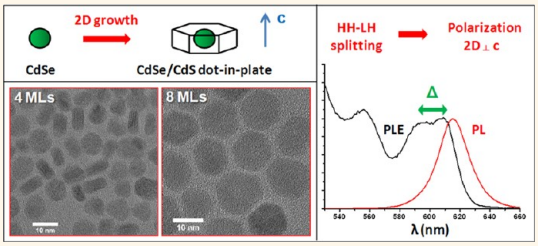

We report the synthesis and properties of a novel class of nanocrystals with mixed dimensionality: a dot-in-plate core/shell nanostructure. This system was synthesized by growing a flat, disk-shaped, CdS shell on spherical CdSe cores. The anisotropic pressure induced by the shell drastically splits the first exciton fine structure in two: the "heavy hole" and "light hole" states become separated by up to 65 meV. As a result, these nanocrystals exhibit an emission strongly polarized in two dimensions, in the plane perpendicular to the wurtzite crystal *c* axis. We use polarization measurements on single nanocrystals and ensemble anisotropy studies to confirm the nature and position of the excitonic energy levels. These nanocrystals orient spontaneously when evaporated on a substrate, enabling a precise control of the orientation of their emission dipole.

KEYWORDS: oblate core/shell nanocrystals · heavy hole to light hole band splitting · 2D polarization · anisotropic pressure · spontaneous orientation

The optical properties of semiconductor nanocrystals (NCs) can be finely tuned by the choice of material composition, size, crystallographic structure, and shape. In particular, design of core/shell NCs provides tunable emission wavelengths over wide ranges of color,[1,2] strongly polarized emission dipole,[3−5] control over the radiative decay rates,[6−8] and the possibility to arrange them into organized superstructures.[9−12]

Since the crystal dimensionality plays a major role on the nanostructure optical properties, the effect of the shape of core and core−shell NCs has been the focus of considerable fundamental and applied research effort. Dot-in-rod and rod-in-rod systems composed of wurtzite materials have been particularly studied. The synthesis of such anisotropic colloidal nanostructures became possible thanks to the high affinity of phosphonic ligands for crystal faces perpendicular to the crystal *c* axis, which induces an important difference in growth kinetics between the *c* axis and the perpendicular directions.[3,13−15]

This 1D anisotropy has a strong influence over the first exciton fine structure of these semiconductor NCs. It has been shown, for example, that the anisotropic shape of CdSe nanorods induces a rearrangement of the electronic states that promotes emission from the linear dipole transition along the rod axis (from the 0^b state).[4,16] It has been also shown that in dot-in-rod NCs with the hole confined in the initial spherical cores, the anisotropic shape also induces the same polarization property. It has been proposed that the shell, mostly grown along the *c* axis, induces an anisotropic pressure due to the lattice mismatch between the core and the shell materials, which affects the first exciton fine structure.[15] To the best of our knowledge, the effect of this anisotropic pressure has, however, not been clearly isolated yet from the dielectric effect of the anisotropic shape which takes an important part in the absorption and emission polarization properties.[5,16,17]

In contrast to 1D-shaped NCs, only a few syntheses of oblate (flat)-shaped colloidal semiconductor NCs have been reported yet. For example, extremely thin (few monolayers) quasi-2D II−VI NCs were reported: nanoplatelets, with a zinc blende structure,[6,18] and nanoribbons, with a wurtzite structure.[19−22] So far, no shell growth has been reported on these objects.

* Address correspondence to thomas.pons@espci.fr, benoit.dubertret@espci.fr.

Received for review March 30, 2012 and accepted July 16, 2012.

Published online July 16, 2012
10.1021/nn3024255

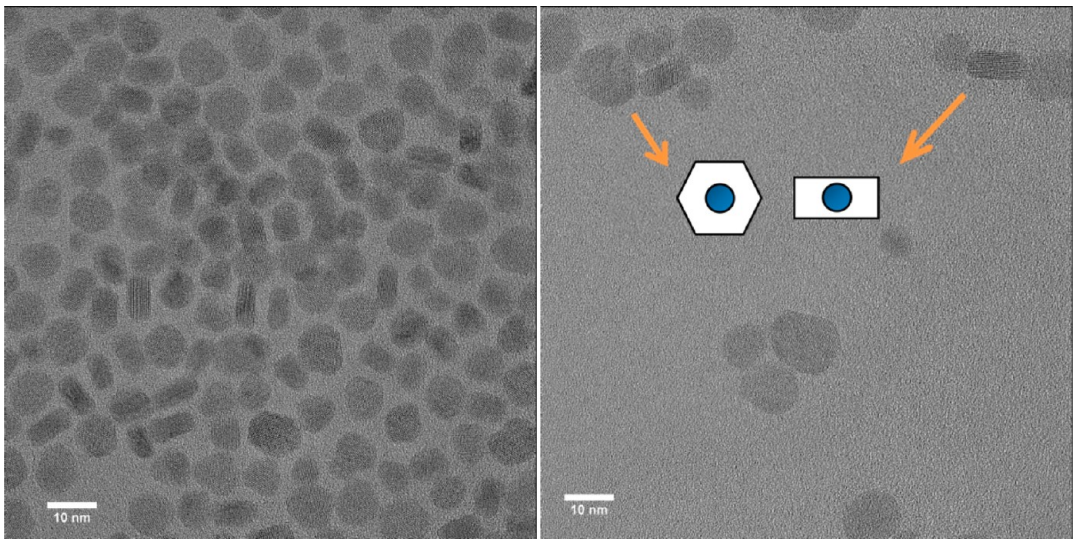

Figure 1. TEM pictures of CdSe/CdS dot-in-plate NCs of 4 (left panel) and 6 (right panel) equivalent CdS monolayers on 1.62 nm cores (samples P4 and P6), with a schematic representation of NCs flat on the grid or on the edge.

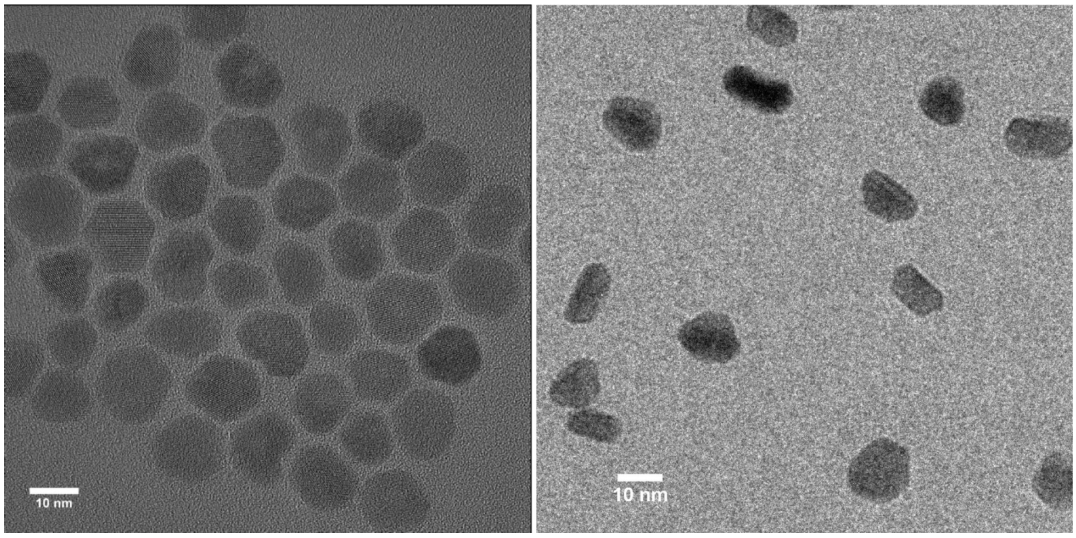

Figure 2. TEM (left panel) and cryo-TEM (right panel) pictures of CdSe/CdS dot-in-plate NCs with 8 equivalent CdS monolayers (sample P8).

In this paper, we report the synthesis of "dot-in-plate" NCs obtained by growing an oblate CdS shell on spherical CdSe cores. Even though the low lattice mismatch between these two semiconductors allows growing "giant shells",[23,24] the pressure induced by the shell on the core is not negligible. Here, we show that the pressure of the anisotropic shell on the spherical core splits the first exciton fine structure in two distinct transitions at room temperature and provides emission polarized in 2D, in the plane of the flat shell. Moreover, we show that these CdSe/CdS dot-in-plate NCs spontaneously deposit flat on different substrates, allowing a precise control of crystalline and dipole orientations.

RESULTS AND DISCUSSION

Shape-Controlled Synthesis. The spherical CdSe cores were made by a modification of Qu *et al.*'s synthesis (see the detailed synthesis in Materials and Methods).[25,26] The synthesis was stopped when the first exciton peak reached 555−560 nm, corresponding to a NC radius of ∼1.55−1.65 nm.[27] The emission peak was shifted from the first exciton absorption peak by approximately 12 nm (global Stokes shift), and its full width at half-maximum (fwhm) of 25−26 nm indicated a good monodispersity. The wurtzite structure of these CdSe cores was confirmed by XRD measurement, with the characteristic peaks at 35.1 and 45.8° (corresponding to (1,0,2) and (1,0,3) planes, respectively, for Cu Kα source; see below).

Different CdS shell sizes were grown on these CdSe cores using two different SILAR (successive ion layer adsorption and reaction)[28] protocols, based on slow and successive injections of metal and sulfur precursors. These two protocols yielded different shell

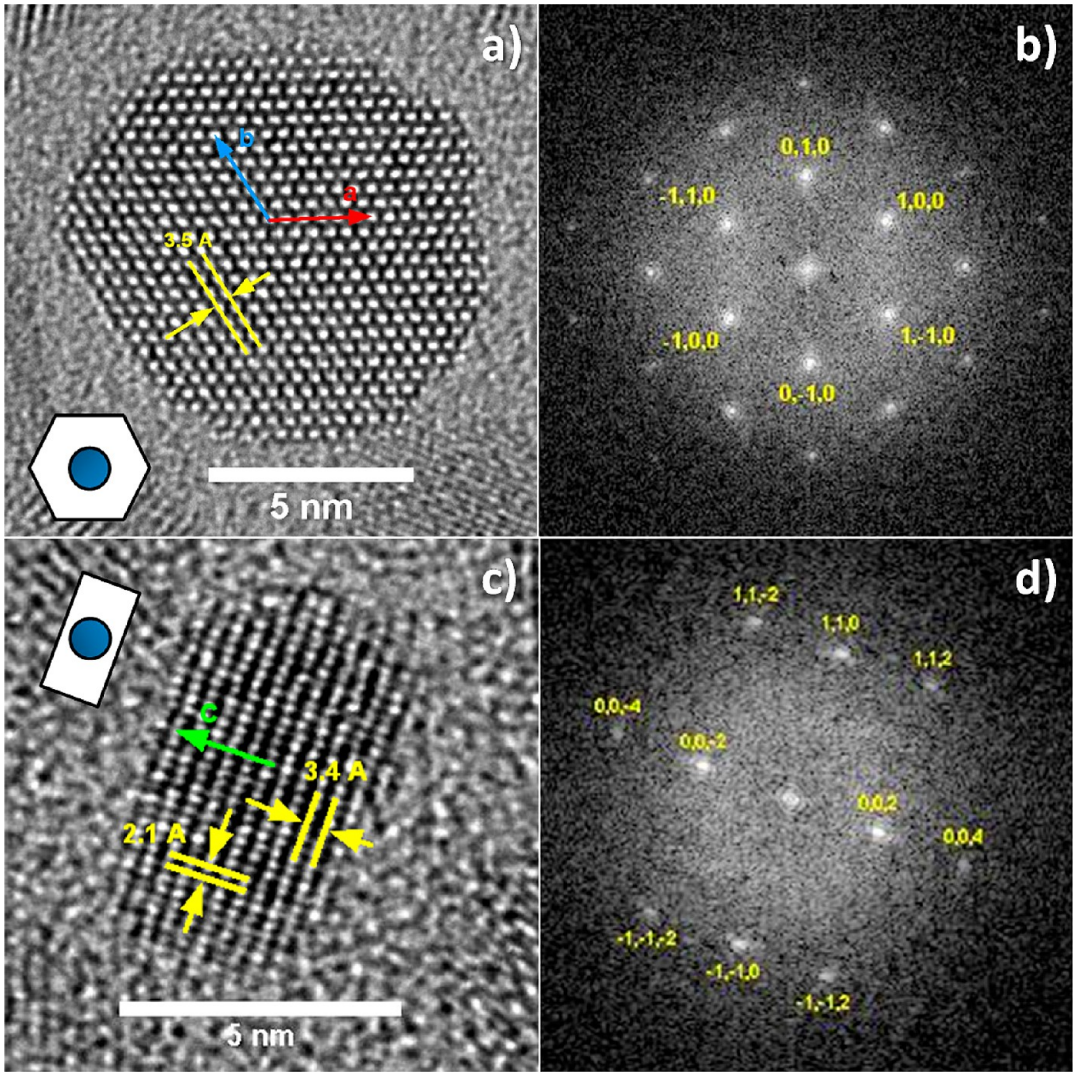

Figure 3. Left panels: HR-TEM picture of CdSe/CdS dots-in-plates with 4 CdS equivalent monolayers on 1.62 nm cores (sample P4), (a) flat on the substrate, (c) lying on the edge in the side. Right panels: corresponding FFT patterns, (b) zone axis [0,0,1], (d) zone axis [−1,1,0].

geometries, as will be demonstrated below. The standard protocol S involved a preparation of cadmium oleate ($Cd(OA)_2$) precursor at 160 °C, a shell synthesis at 260 °C, starting with S injection, and yielded spherical shells. In contrast, protocol P resulted in oblate CdS shells and involved a preparation of $Cd(OA)_2$ precursor at much higher temperature (300 °C) and shell synthesis at 230−240 °C, starting with Cd injection (see experimental details in Materials and Methods).

Usually, wurtzite II−VI NCs tend to grow with slightly prolate shapes along the crystal *c* axis (aspect ratio ~1.1:1 or above[29,30]). However, in protocol P, the growth was quasi-two-dimensional, preferentially along directions perpendicular to the *c* axis (see below), and resulted in NCs with dot-in-plate geometry. This difference of growth kinetics could be explained by different causes, including a possible degradation of oleic acid or its impurities at elevated temperatures. These reactions could lead to a modification of the $Cd(OA)_2$ reactivity or to the apparition of ligands capable of specifically binding to the (0,0,1) and the (0,0,−1) facets and thus strongly reducing the shell growth along the *c* direction. The shell synthesis temperature also has a strong influence on the growth. We observed that high (260 °C) temperatures resulted in a more isotropic growth and yielded spherical-shaped QDs. In contrast, temperatures of 200 to 240 °C can be used to synthesize dot-in-plate NCs.

Structural Characterization. Structural characterizations of CdSe/CdS core/shell NCs obtained from protocols S and P were performed by TEM and cryo-TEM measurements. Protocol S yielded perfectly isotropic NCs in both TEM and cryo-TEM pictures that were consistent with a spherical NC shape (sample S6 in Figure S2 in Supporting Information). In contrast, the anisotropic shape of NCs made by the protocol P was clearly seen in TEM for CdS shell thicknesses corresponding to an equivalent of 3 monolayers or more.

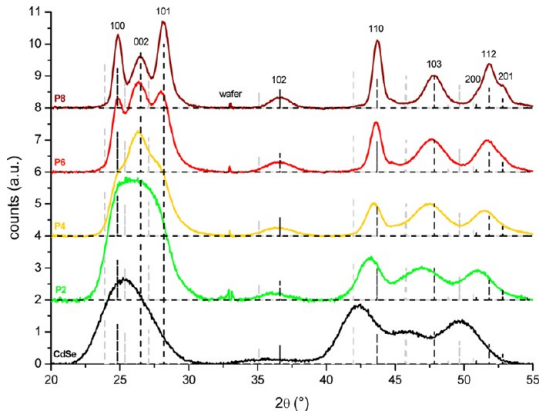

Figure 4. XRD profiles of CdSe cores (black line), CdSe/CdS dot-in-plate NCs with 2, 4, 6, and 8 equivalent CdS monolayers (green to brown line). Black (gray) dashed lines represent theoretical bulk wurtzite CdS (CdSe) pattern (PDF nos. 00-008-0459 and 00-041-1049), with the corresponding *h*,*k*,*l* numbers.

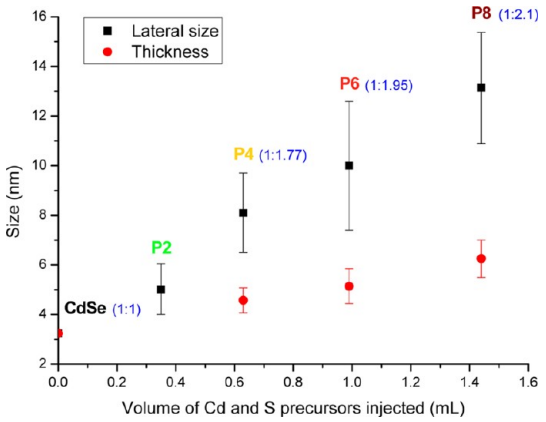

Figure 5. Lateral sizes (black) and thicknesses (red) of CdSe cores and corresponding CdSe/CdS dot-in-plate NCs with 2, 4, 6, and 8 equivalent CdS monolayers. Sample aspect ratios were added in blue.

For example, Figure 1 shows dot-in-plate NCs corresponding to 4 and 6 equivalent CdS monolayers (samples P4 and P6) lying flat on the grid or standing on their edge. For larger shells, dot-in-plate NCs were all lying flat on the grid, but the flat anisotropic shape was confirmed in cryo-TEM where NCs were frozen in water in random orientations (Figure 2). In addition, TEM pictures show that NCs synthesized using protocol P were hexagonally faceted.

The crystal orientation was deduced from the fast Fourier transform (FFT) of high-resolution TEM (HR-TEM) pictures. For crystals lying flat on the grid, as shown in Figure 3 (top panel), the FFT pattern has an hexagonal symmetry with 60° angles and the distance measured between the fringes, 3.5 Å, was in good agreement with the [0,0,1] CdS zone axis (1.2% error). This indicates that, in these NCs, the crystal *c* axis is perpendicular to the picture plane. In contrast, when the crystals were on their edge, two arrays of fringes were observed with 90° angles (Figure 3 (bottom panel). The spacing of the fringes perpendicular to the crystal thickness direction was 3.4 Å, and we measured 2.1 Å in the other direction. These parameters were consistent with a [−1,1,0] CdS zone axis (0.9 and 0.5% error, respectively). Taken together, these orientations show that the *c* axis is parallel to the crystal thickness direction and that the *a* and *b* axes point toward the hexagonal vertices. The shell growth therefore occurred mostly in the (*a*,*b*) plane of the wurtzite structure and was strongly reduced along the *c* axis.

This structure was confirmed by examination of XRD profiles of CdSe/CdS dot-in-plate NCs at different shell growth stages, as shown in Figure 4. The peaks shifted from the position of the bulk wurtzite CdSe (gray dashed peaks) to those of the pure CdS (black dashed peaks), as the thickness of the CdS shell increased. At the same time, their widths gradually decreased inversely proportionally to the NC thickness along the corresponding directions, according to the Scherrer's formula (see Materials and Methods). Peaks corresponding to directions in the (*a*,*b*) plane, such as (1,0,0) and (1,1,0), were noticeably thinner than other peaks with contributions in the *c* direction (*i.e.*, (0,0,2), (1,0,3), (1,1,2), *etc.*), in agreement with a shell growing preferentially in the (*a*,*b*) plane compared to the *c* direction.

Figure 5 shows the lateral size (in black) and thickness (in red) of the different dot-in-plate samples, made by protocol P. The CdSe core size was calculated from literature.[27] The lateral size of P2, P4, P6, and P8 and the thickness of P4 and P6 were directly measured by TEM (histograms in Figures S4 and S5 in Supporting Information). However, the thickness of P8 sample was estimated from the peak widths of its XRD profile (Figure S6 in Supporting Information) since all NCs from this sample laid flat on the TEM grid. The dispersity of dot-in-plate NC lateral sizes was quite important, around 20%. The aspect ratio of dot-in-plate samples increased up to ∼1:2 during the shell growth (Figure 5, blue numbers), which means that the growth was anisotropic during the whole shell synthesis.

The localization of the CdSe core in the center of the plate (*a*,*b*) plane, expected from the crystal symmetry, was confirmed using scanning TEM/energy-dispersive X-ray (EDX) spectroscopy measurements (see Figures S7 and S8 in Supporting Information). In addition, geometrical phase analysis (GPA) on high-angle annular dark-field (HAADF) scanning TEM images shows a deformation of the lattice around the center of the dot-in-plate heterostructures, on the order of 3−5% (see Figure S9 in Supporting Information). This corresponds to the expected lattice mismatch between CdSe and CdS and confirms that the CdSe core is localized in the center of the dot-in-plate (*a*,*b*) plane. On the other hand, we note that the reactivity of (001) and (00−1) facets may be different,[10,31] and thus growth of the CdS along the *c* direction may be slightly asymmetric in the dot-in-plate samples.

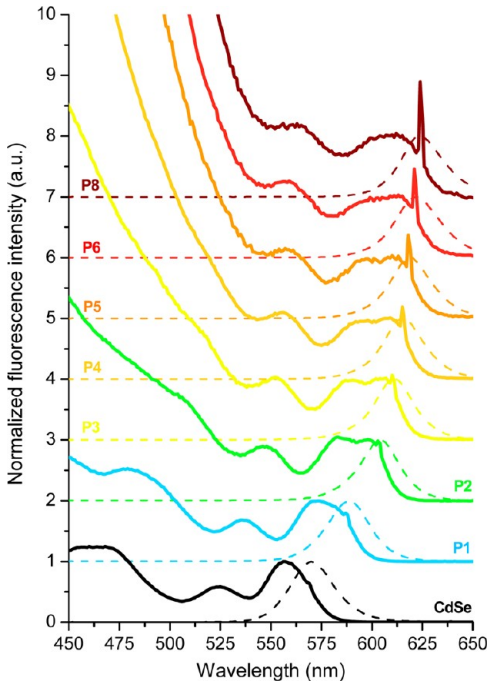

Figure 6. PLE (solid lines) and PL (dashed lines) spectra during the anisotropic shell growth, normalized to the first exciton peak. Initial CdSe core (r = 1.62 nm) spectra are in black, and the lines from blue to brown represent the different shell sizes (1−6, 8 equivalent CdS monolayers). The sharp peaks in PLE spectra correspond to the scattered light at the detection wavelength.

Optical Properties. For both spherical and oblate shells, the growth of CdS on the spherical CdSe cores was followed by monitoring the photoluminescence (PL) and photoluminescence excitation (PLE) spectra (Figures 6 and S10 and S11 in Supporting Information). The spectra shift to redder wavelengths when the number of CdS monolayers increases, according to the delocalization of the electron in the entire NC (the hole remained localized in the core). Simultaneously, the portion of the PLE (and absorption) at high energy (<500−520 nm) increases due to the shell contribution (Figure S10).

The widths of the PL spectrum and of the PLE first exciton peak, as well as the Stokes shift, remained almost unchanged during shell growth for spherical CdSe/CdS NCs (Figure S11 in Supporting Information). In contrast, for CdSe/CdS dot-in-plate NCs, the global Stokes shift drastically decreased from ∼50 to 17 meV and the fwhm of the emission narrowed down to 23 nm (Figure 6). Simultaneously, the first exciton peak in PLE (and in absorption) progressively split into two transitions, starting from 1 equivalent CdS monolayer.

In II−VI NCs, the first exciton ($1S_{3/2}-1S_e$[32]), which is responsible for the emission, is split into five energy levels by the crystal anisotropy (internal structure and shape asymmetries) and the electron−hole exchange interaction.[33] In spherical or slightly prolate wurtzite CdSe NCs, this fine structure cannot be resolved at room temperature. The exchange interaction term is expected to decrease with the growth of CdS on CdSe due to the reduction of the electron and hole wave function overlap.[7,33] The anisotropy term, noted Δ, separates the heavy hole and light hole bands (HH and LH, respectively) and depends on the shape, the aspect ratio, and the ratio of the light to heavy hole effective masses.[33]

Here we attributed the splitting of the first excitonic peak during the shell growth to the anisotropic pressure of the CdS shell on the CdSe cores, which induced an additional splitting between the heavy hole and light hole bands. Similar splitting was reported for epitaxially grown quantum dots (see, for example, refs 34 and 35). In the case of CdSe/CdS core/shell NCs, with a lattice mismatch about 3.8%, we used a cylinder-in-a-cylinder geometry to model the anisotropic pressure in our dot-in-plate system, and we neglected the amount of CdS grown along the c axis. Within these approximations, we calculated the evolution of the heavy hole (HX) and light hole (LX) exciton splitting ($E_{LX}-E_{HX}$) during the shell growth (see Supporting Information for the definition of LX and HX excitons and for the theoretical estimation of their splitting, Figure S13).[36,37] In good agreement with the model, Figure 6 shows a rapid increase of the splitting due to the pressure buildup, which rapidly saturates after a few monolayers, up to ∼65 meV for the sample P4, compared to ∼77 meV predicted theoretically using a cylindrical instead of spherical core. The splitting decreases slightly for the largest shell sample (sample P8, Figures 6 and S13). This might be due to the small amount of CdS shell deposited on the (0,0,1) and/or (0,0,−1) faces, which reduces the pressure asymmetry on the core. However, even for this sample, the splitting is still large enough to separate the light and the heavy hole bands by around 60 meV. In addition, for this sample, the global Stokes shift slightly increases from ∼17 to ∼20 meV (Figure 6). This might be attributed to increased phonon interactions due to the reduction of the electron and hole wave function overlap.[38,39] It could also result from a size distribution broadening in the thickness direction as the CdS shell grows.

To confirm the role of the pressure on this splitting, we have grown a shell of a semiconductor with a higher lattice mismatch, using an alloy between CdS and ZnS (ZnS has a 12% lattice mismatch with CdSe). The synthesis was made in the same condition as for CdSe/CdS dot-in-plate NCs, but we increased progressively the proportion of ZnS in the shell (see details in Materials and Methods). The splitting then increased up to ∼70 meV (Figure S12 in Supporting Information), while the PL fwhm remained at 25 nm. The growth of a CdZnS alloy shell effectively induced higher anisotropic pressure. However, the shape of these CdSe/CdZnS dot-in-plate NCs was not as well-defined as CdSe/CdS dot-in-plate NCs (Figure S3 in Supporting Information).

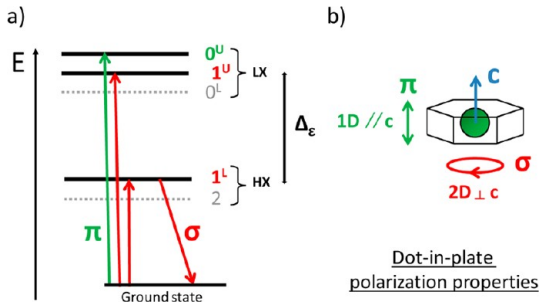

Figure 7. (a) Schematic of energy levels in CdSe/CdS dot-in-plate NCs; (b) orientation of the corresponding transition polarizations with respect to the crystallographic structure. Green arrows represent transitions polarized linearly along the *c* axis. Red arrows represent transitions polarized in the (*a*,*b*) plane.

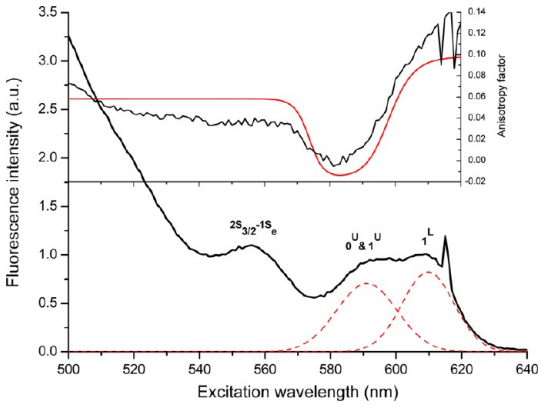

Figure 8. Top graph: anisotropy factor (*R*) *vs* excitation wavelength; in black, experimental results on dot-in-plate NCs with 4 equivalent CdS monolayers on 1.62 nm cores (sample P4); in red, calculated *R* (no adjustable parameters). The corresponding PLE spectrum is shown below and was fitted by Gaussians for theoretical prediction (red dashed lines).

We now examine the effect of the heavy hole and light hole splitting on the optical properties of the NC emission. In II−VI NCs, the 8-fold degenerated first exciton is split into five energy levels.[33] Two of them, $F_m = \pm 2$ and 0^L are optically passive (their oscillator strengths are zero) and do not participate in the absorption nor in the emission at room temperature. The energy levels and oscillator strengths of the three optically active ones, the 0^U, $\pm 1^U$, and $\pm 1^L$ states, control the properties of the NC emission, in particular, their polarization. In wurtzite structures, the transitions between the $\pm 1^U$ or $\pm 1^L$ states and the (no exciton) ground state are circularly polarized in the (*a*,*b*) plane (σ transitions). In contrast, the 0^U to ground state transition is linearly polarized along the *c* axis (π transition).[33] In our CdSe/CdS dot-in-plate NCs, the splitting between the HH and LH bands induces a separation of the first exciton into two separate groups: the "LX transition" containing the 0^U, 0^L, and $\pm 1^U$ states and the "HX transition" containing the $\pm 1^L$ and ± 2 states. In contrast to CdSe cores in which this splitting is on the order of 20 meV (for radius ~1.5 nm, depending on the core shape), the LX−HX splitting becomes much larger than *kT* at room temperature for our dot-in plates NCs. As a consequence, in these nanostructures, PL emission should come only from the lower $\pm 1^L$ states and should therefore be polarized in the 2D plane of the shell, perpendicularly to the *c* axis (see the schematics in Figure 7).

To confirm the identification of these transitions and the 2D-polarized emission of dot-in-plates NCs, we measured their excitation anisotropy spectrum.[40] The anisotropy factor *R*, given by the equation SE1 in Supporting Information, was measured by recording the integrated photoluminescence excitation spectra (IPLE) of dot-in-plate NCs in viscous solution, for all combinations of horizontal or vertical polarizers placed in the excitation and detection path of a fluorescence spectrometer (see Supporting Information for experimental details). This allows us to determine an excitation wavelength-dependent anisotropy factor, $R(\lambda_{exc})$, which is related to the angle between the absorption and the emission dipoles.[40] In particular, the anisotropy factor should be zero when the absorption transitions are completely isotropic, negative when the emission dipole is perpendicular to the excitation dipole, and positive when they are parallel. In the case of our CdSe/CdS dot-in-plate NCs with 2D emission polarization, *R* is expected to vary between −0.2 and 0.1 (see Supporting Information for theoretical details).

The experiments were performed on dot-in-plate NCs with 4 equivalent CdS monolayers on 1.62 nm cores (sample P4), and the corresponding experimental anisotropy spectrum, $R(\lambda_{exc})$, is represented in Figure 8, top black line. The resulting curve is consistent with our theoretical expectations (red curve, Figure 8) derived from a fit of the PLE spectrum and the theoretical anisotropy factors for each transition (see Figure S17 in Supporting Information). The maximum of *R* was obtained when we excited at the band edge (~600−610 nm) and was close to the theoretical value of 0.1 when the excitation and the emission involve the same $\pm 1^L$ states (2D-polarized transitions). In contrast, a completely isotropic transition would yield a zero anisotropy factor (see anisotropy spectrum of spherical core/shell NCs in Figure S16 in Supporting Information), while a 1D transition would yield an anisotropy factor of 0.4.[40] At lower energy, the anisotropy factor continued to increase. This was attributed to beam scattering and to the very low signal-to-noise ratio at these low excitation energies.[40] At higher excitation energy, up to ~580 nm, the anisotropy factor drastically decreased to approximately zero, corresponding to excitation of the "LX" transitions which contain contributions from the 0^U state (π-polarized, along the *c* axis, $R = -0.2$) and from the $\pm 1^U$ states (2D-polarized, $R = 0.1$), weighted by their respective oscillator strengths (see Supporting Information). Finally, the positive anisotropy factor at higher energies (starting with $2S_{3/2}-1S_e$ transition) revealed the role

of the shape effect in the excitation process; this dielectric effect reduced the excitation field along the *c* axis inside the NC, while it exalted the field polarized in the plate plane.[41] This shape effect has been previously observed in quantum rods or nanowires[5,17] and leads to a constant positive anisotropy, consistent with predicted values (see Supporting Information for theoretical details). We attribute the deviations between the experimental and theoretical excitation anisotropy spectra near the "LX" transition to nonzero electron−hole exchange interaction in this sample, in contrast to what was assumed for theoretical predictions for simplicity. This would induce a small separation between the 0^U and $\pm1^U$ states and modify their respective oscillator strengths compared to those assumed (2/3 and 1/3, respectively;[33] see Supporting Information). Deviations (~0.02) between theoretical and experimental anisotropy spectra at lower excitation wavelengths could be tentatively attributed to the wavelength dependence of the CdS refractive index, an inaccurate instrumentation factor (*G*) measurement, and/or to the approximation of the NC shape by an oblate ellipsoid (see Supporting Information). Overall, these results confirm the separation of the LH and HH bands in these dot-in-plates NCs, the nature of each transition in the first exciton fine structure, and the 2D polarization of the emission.

We further confirmed the 2D nature of the emission polarization by polarization measurements on single NCs in thick films using fluorescence microscopy.[42] Dot-in-plate NCs were spin-coated in a polymer solution on a glass coverslip to provide 3D random orientation. Their emission was then separated into two perpendicular (*x* and *y*) polarization components in the image plane and recorded simultaneously on a CCD camera to provide single NC polarization-resolved intensities, I_x and I_y (see schematic in Figure S18 in Supporting Information). The resulting histogram of polarization degrees, $I_x/(I_x + I_y)$, is consistent with the 2D nature of the emission polarization from the $\pm1^L$ states (see Figure S19 in Supporting Information).

In addition to these novel polarization properties, these dot-in-plates NCs deposit in a controlled orientation on flat substrates. TEM pictures of dot-in-plate samples in Figures 1 and 2 show NC tendency to lie down flat on the TEM carbon layer (*i.e.*, with the *c* axis perpendicular to the substrate plane), and this effect is progressively more pronounced as the number of CdS monolayers increased. In particular, all isolated NCs deposited flat on the carbon layer, while the majority of the NCs oriented on the edge were surrounded by other NCs. This indicates that their oblate shape, with an aspect ratio around 1:2, favored their deposition parallel to the substrate, while deposition on the edge could be due to interactions with the neighboring NCs. For the sample with 8 equivalent CdS monolayers, all NCs were found flat on the grid (Figure 2, left), and we expect that, for relatively dilute solution, it would be the same for a large variety of substrates.

We tested this controlled orientation by drying a drop of diluted dot-in-plate NCs on glass coverslips and measuring their radiation diagram (see Supporting Information). As the transition dipoles in these NCs are defined by their orientation relative to the crystal *c* axis (see above and Figure 7), their spontaneous orientation on the substrate leads to a controlled orientation of their dipoles. When compared to isotropic emission of spherical zinc blende CdSe/CdS NCs, dot-in-plate NCs exhibited a radiation diagram with a maximum emission along the direction perpendicular to the substrate, as expected from 2D-polarized emitters oriented parallel to the substrate (Figure S20 in Supporting Information).

CONCLUSION

To conclude, we have described the synthesis of core/shell dot-in-plate nanocrystals by growing an oblate CdS shell on spherical CdSe cores, with a SILAR protocol. The difference of growth kinetics between the crystal directions along and perpendicular to the *c* axis lead to dot-in-plate NCs with a final aspect ratio around 1:2. The anisotropic pressure induced by the shell strongly affects the first exciton fine structure which splits in two, while the PL fwhm narrows to 23 nm. This splitting, between the light and heavy hole bands, as well as the dielectric effect due to the shape anisotropy, induces an emission polarization of theoretically ~98% in two dimensions (see Supporting Information), in the plane perpendicular to the *c* axis of the wurtzite NC structure. Moreover, this new core/shell nanostructure spontaneously aligns in a controlled crystalline orientation when deposited on a substrate. This latter property is particularly interesting for applications relying on exciton/exciton or exciton/plasmon coupling which require a fine control over dipole orientations. Fundamental studies could also benefit from controlled orientation, such as spin interactions with external magnetic fields. Indeed, it has been theoretically predicted that magnetic field applied along the *c* direction of the NCs should only split the states with degenerated total spin, without any state mixing.[33]

MATERIALS AND METHODS

Chemicals. Cadmium oxide (CdO, 99.99%), zinc oxide (ZnO, 99%), selenium pellets (Se, 99.99%), sulfur powder (S, 99.998%), 1-octadecene (ODE, 90%), oleic acid (OA, 90%), hexadecylamine (HDA, 90%), octylamine (99%), and polybutadiene were purchased from Sigma-Aldrich. We used a technical grade trioctylphosphine (TOP, 90%) purchased from either Sigma or Cytop-380 (TOP, >95%), a gift from Cytec. Trioctylphosphine oxide (TOPO, 90%) Cyanex-921 was also a gift from Cytec. These chemicals were used as provided without further purification. Se and TOP were stored under Ar atmosphere. Oleylamine (OAm, >70%), purchased

from Fluka, was centrifuged to remove a small amount of precipitate.

Preparation of the Precursors. *Cadmium Oleate ($Cd(OA)_2$) 0.5 M in OA and 0.1 M in OA/ODE.* CdO and OA (1:6) were heated at 160 °C under Ar, until the solution became colorless. The $Cd(OA)_2$ solution was then degassed at 80 °C to remove water. For asymmetric growth of CdS, the CdO and OA solution was heated at 300 °C and kept at this temperature for ~1 h. In both cases, the waxy $Cd(OA)_2$ solution was diluted in ODE (1:4 in volume) to be used for CdS growth.

Zinc Oleate ($Zn(OA)_2$) 0.5 M in OA and 0.1 M in OA/ODE. The protocol for $Zn(OA)_2$ preparation was identical to that of $Cd(OA)_2$ except that the ZnO and OA solution was always heated at 280−300 °C for 1 h to obtain a clear solution. The solution was also diluted in ODE (0.1M) for the ZnS shell growth.

Solution of Sulfur in ODE (S(ODE)) 0.1 M. ODE was degassed at 70 °C for 30 min. Sulfur powder was then introduced under argon, and the solution was heated at 180 °C until complete dissolution.

Solution of Selenium in TOP ((TOP)Se) 1 M. (TOP)Se 1 M was prepared in a glovebox under Ar atmosphere by dissolving selenium pellets in TOP under magnetic stirring.

Nanocrystal Synthesis. *CdSe Core Synthesis.* First, 750 μL of $Cd(OA)_2$, 0.5 M in OA, was introduced in a three-necked flask with 1.3 mL of TOPO and 5 mL of ODE. The mixture was degassed at 70 °C for at least 30 min. Under Ar, a solution of 3 mL of OAm and 4 mL of (TOP)Se 1 M was quickly injected at 300 °C, and the temperature was set at 280 °C for typically 2−6 min of reaction. The solution was then cooled to room temperature, and the nanocrystals were washed by precipitation with ethanol followed by redispersion in hexane.

Spherical CdS Shell Growth (Protocol S). Two milliliters of ~80 μM (see Supporting Information for concentration measurement) of CdSe cores was introduced in a flask with 5 mL of ODE and 1 mL of HDA, and the mixture was degassed for 30 min at 70 °C. Under argon, the solution was heated to 100 °C and a volume of S(ODE) 0.1 M, corresponding to the first monolayer of CdS, was injected dropwise at this temperature (see Supporting Information for the calculation of Cd and S solution volumes). The temperature was increased to 260 °C, and we injected dropwise the $Cd(OA)_2$ 0.1 M OA/ODE made at 160 °C and the S(ODE) 0.1 M, successively. We waited 5 min after the introduction of the cadmium, whereas the sulfur was allowed to react for at least 10 min. Few changes were visible in PL and PLE spectra after the injection of Cd, whereas changes in optical properties occurred after S introduction. We finished the synthesis with an injection of excess $Cd(OA)_2$ 0.1 M OA/ODE to provide a good stability of the NCs and a better fluorescence quantum yield. At room temperature, we added a few milliliters of octylamine to improve the solubilization of the nonreacted carboxylates, and the NCs were washed with ethanol.

Flat CdS Shell Growth (Protocol P). CdSe/CdS dot-in-plate NCs were synthesized using a variation of the procedure used for spherical CdSe/CdS NCs. A batch of NCs with different shell sizes was made on initial CdSe cores of 1.62 nm in radius. In a flask, 1 mL of HDA and 5 mL of ODE were mixed with 2 mL of CdSe NCs in hexane (~80 μM) and degassed at 70 °C for 30 min. The solution was heated at 230 °C and the first Cd volume of $Cd(OA)_2$, 0.5 M prepared at 300 °C and diluted in ODE (0.1M), was dropwise injected. After 15 min of reaction, S(ODE) 0.1 M was injected dropwise and the temperature was increased to 240 °C. Every 15 min, the Cd and S precursor solutions were injected. The temperature was maintained at 240 °C. After the last deposited S monolayer, the NCs were washed like the spherical ones.

The CdSe cores can also be introduced after the first Cd injection to reduce their partial dissolution when heated at 230 °C with primary amine. This helps to avoid homogeneous nucleation of CdSeS particles. If some of these smaller particles were formed during the shell growth, they were removed by size-selective precipitation with butanol.

CdZnS Gradient Shell Growth on Dot-in-Plate NCs. The protocol was identical to that used for CdSe/CdS dot-in-plate synthesis. The CdSe cores (1.59 nm in radius) were introduced at room temperature with ODE and HDA. We first deposited 2 equivalent monolayers of CdS using the Cd solution made from $Cd(OA)_2$ synthesized at 300 °C. For the other layers, we used a mixture of $Cd(OA)_2$ and $Zn(OA)_2$ 0.1 M, with progressively larger Zn/Cd ratio (2 monolayers at a 1:2 ratio, then 2 monolayers at 1:1, then 2 monolayers at 2:1).

Structural Characterizations. For all TEM measurements, the samples were washed by several cycles of precipitation/redispersion, successively with ethanol, acetone, and isopropyl alcohol.

TEM and HR-TEM. TEM and HR-TEM images were recorded on ultrascan 4k CCD camera (Gatan, USA), using a JEOL 2100F (JEOL, Japan) with a field emission gun (FEG) operating at 200 kV.

For the determination of the interplane distances, we used the fast Fourier transform (FFT) of a selected NC in the HR-TEM picture and the CaRIne software for identification, using the lattice parameters of CdS (a = 4.135 Å, c = 6.749 Å). Distance calibration was performed on carbon graphite at 400k and 600k magnifications.

Cryo-TEM. Spherical and dot-in-plate NCs were transferred into water before cryo-TEM measurements using ligand exchange with dihydrolipoic acid/sulfobetaine ligands as previously reported by Muro *et al.*[43] A drop of NC dispersion was deposited on Quantifoil (Quantifoil Micro Tools Gmbh, Germany) carbon membrane. The excess of liquid on the membrane was blotted out with a filter paper, and before evaporation, the membrane was quench-frozen in liquid ethane to form a thin vitreous ice film. Once mounted in a cryo-holder cooled with liquid nitrogen, the samples were transferred in the microscope and observed at low temperature (−180 °C). Since this method yields NCs frozen in solution, we were able to observe them in all orientations. Images were recorded on ultrascan 2k CCD camera (Gatan, USA), using a LaB_6 JEOL 2100 (JEOL, Japan) cryo-microscope, operating at 200 kV with a JEOL low-dose system (minimum dose system, MDS) to protect the thin ice film from any irradiation before imaging and reduce the irradiation during the image capture.

XRD Measurement. Drops of highly concentrated solution of nanocrystals were deposited on a Si wafer. Powder X-ray diffraction (XRD) patterns were acquired using a Philips X'Pert diffractometer with a Cu Kα source and an Xcelerator detector. XRD profile of sample P8 (8 equivalent CdS monolayers on 1.62 nm cores) was corrected from background and fitted using pseudo-Voigt functions. We then used Scherrer's formula (see below) to determine the NC thickness. Here we neglected the effect of strains on the peak broadening, and the factor k was used as for spherical NCs for simplicity.

$$d_{hkl} = \frac{k\lambda_{K\alpha}}{\mathrm{fwhm}_{hkl}\cos(\theta_{hkl})}$$

where d_{hkl} is the size of the NCs along the direction perpendicular to the (h,k,l) plane; k = 0.89 is a constant; $\lambda_{K\alpha}$ is the wavelength of the Cu Kα X-ray source; fwhm_{hkl} is the width of the h,k,l peak; and θ_{hkl} is the diffraction angle.

Optical Characterizations. All optical measurements were performed at room temperature with NCs dispersed in hexane except for ensemble anisotropy measurements. Absorption measurements were carried out with a Cary 5E UV−vis−NIR spectrophotometer (Varian). Photoluminescence (PL), photoluminescence excitation (PLE), and integrated photoluminescence excitation (IPLE) spectra were acquired using a FCS900 spectrometer (Edinburgh Instruments) equipped with a R928P photomultiplier and a white Xe lamp. PL and PLE spectra of QD solutions were recorded with optical densities below 0.1 at 400 nm and corrected by the excitation intensity and detector sensitivity.

Conflict of Interest: The authors declare no competing financial interest.

Acknowledgment. We acknowledge the Agence Nationale pour la Recherche (ANR) for financial support, A. Fragola for assistance with single QD polarization and radiation diagram experiments, N. Lequeux and P. Bassoul for crystallographic discussion, and C. Delerue for discussion on phonons.

Supporting Information Available: Detailed syntheses, preparation of samples; complementary TEM and cryo-TEM pictures;

size measurements; description of instrumentation; complementary PL and PLE spectra; EDX-STEM measurements; GPA; model of strain; single polarization measurement; fluorescence anisotropy principle and calculation including dielectric effect; and diagram of radiation. This material is available free of charge *via* the Internet at http://pubs.acs.org.

REFERENCES AND NOTES

1. Reiss, P.; Protiere, M.; Li, L. Core/Shell Semiconductor Nanocrystals. *Small* **2009**, *5*, 154–168.
2. Smith, A. M.; Nie, S. M. Semiconductor Nanocrystals: Structure, Properties, and Band Gap Engineering. *Acc. Chem. Res.* **2010**, *43*, 190–200.
3. Peng, X. G.; Manna, L.; Yang, W. D.; Wickham, J.; Scher, E.; Kadavanich, A.; Alivisatos, A. P. Shape Control of CdSe Nanocrystals. *Nature* **2000**, *404*, 59–61.
4. Hu, J. T.; Li, L. S.; Yang, W. D.; Manna, L.; Wang, L. W.; Alivisatos, A. P. Linearly Polarized Emission from Colloidal Semiconductor Quantum Rods. *Science* **2001**, *292*, 2060–2063.
5. Sitt, A.; Salant, A.; Menagen, G.; Banin, U. Highly Emissive Nano Rod-in-Rod Heterostructures with Strong Linear Polarization. *Nano Lett.* **2011**, *11*, 2054–2060.
6. Ithurria, S.; Tessier, M. D.; Mahler, B.; Lobo, R.; Dubertret, B.; Efros, A. Colloidal Nanoplatelets with Two-Dimensional Electronic Structure. *Nat. Mater.* **2011**, *10*, 936–941.
7. Brovelli, S.; Schaller, R. D.; Crooker, S. A.; Garcia-Santamaria, F.; Chen, Y.; Viswanatha, R.; Hollingsworth, J. A.; Htoon, H.; Klimov, V. I. Nano-Engineered Electron−Hole Exchange Interaction Controls Exciton Dynamics in Core−Shell Semiconductor Nanocrystals. *Nat. Commun.* **2011**, *2*, 280.
8. Dorfs, D.; Salant, A.; Popov, I.; Banin, U. ZnSe Quantum Dots within Cds Nanorods: A Seeded-Growth Type-II System. *Small* **2008**, *4*, 1319–1323.
9. Rogach, A. L.; Talapin, D. V.; Shevchenko, E. V.; Kornowski, A.; Haase, M.; Weller, H. Organization of Matter on Different Size Scales: Monodisperse Nanocrystals and Their Superstructures. *Adv. Funct. Mater.* **2002**, *12*, 653–664.
10. Carbone, L.; Nobile, C.; De Giorgi, M.; Sala, F. D.; Morello, G.; Pompa, P.; Hytch, M.; Snoeck, E.; Fiore, A.; Franchini, I. R.; *et al.* Synthesis and Micrometer-Scale Assembly of Colloidal CdSe/CdS Nanorods Prepared by a Seeded Growth Approach. *Nano Lett.* **2007**, *7*, 2942–2950.
11. Murray, C. B.; Kagan, C. R.; Bawendi, M. G. Self-Organization of CdSe Nanocrystallites into 3-Dimensional Quantum-Dot Superlattices. *Science* **1995**, *270*, 1335–1338.
12. Miszta, K.; de Graaf, J.; Bertoni, G.; Dorfs, D.; Brescia, R.; Marras, S.; Ceseracciu, L.; Cingolani, R.; van Roij, R.; Dijkstra, M.; *et al.* Hierarchical Self-Assembly of Suspended Branched Colloidal Nanocrystals into Superlattice Structures. *Nat. Mater.* **2011**, *10*, 872–876.
13. Peng, Z. A.; Peng, X. G. Mechanisms of the Shape Evolution of CdSe Nanocrystals. *J. Am. Chem. Soc.* **2001**, *123*, 1389–1395.
14. Manna, L.; Scher, E. C.; Alivisatos, A. P. Synthesis of Soluble and Processable Rod-, Arrow-, Teardrop-, and Tetrapod-Shaped CdSe Nanocrystals. *J. Am. Chem. Soc.* **2000**, *122*, 12700–12706.
15. Talapin, D. V.; Koeppe, R.; Gotzinger, S.; Kornowski, A.; Lupton, J. M.; Rogach, A. L.; Benson, O.; Feldmann, J.; Weller, H. Highly Emissive Colloidal CdSe/CdS Heterostructures of Mixed Dimensionality. *Nano Lett.* **2003**, *3*, 1677–1681.
16. Shabaev, A.; Efros, A. L. 1D Exciton Spectroscopy of Semiconductor Nanorods. *Nano Lett.* **2004**, *4*, 1821–1825.
17. Wang, J. F.; Gudiksen, M. S.; Duan, X. F.; Cui, Y.; Lieber, C. M. Highly Polarized Photoluminescence and Photodetection from Single Indium Phosphide Nanowires. *Science* **2001**, *293*, 1455–1457.
18. Ithurria, S.; Dubertret, B. Quasi 2D Colloidal CdSe Platelets with Thicknesses Controlled at the Atomic Level. *J. Am. Chem. Soc.* **2008**, *130*, 16504–16505.
19. Joo, J.; Son, J. S.; Kwon, S. G.; Yu, J. H.; Hyeon, T. Low-Temperature Solution-Phase Synthesis of Quantum Well Structured CdSe Nanoribbons. *J. Am. Chem. Soc.* **2006**, *128*, 5632–5633.
20. Li, J. P.; Xu, Y.; Wu, D.; Sun, Y. H. Hydrothermal Synthesis of Novel Sandwich-like Structured ZnS/Octylamine Hybrid Nanosheets. *Solid State Commun.* **2004**, *130*, 619–622.
21. Liu, Y. H.; Wang, F. D.; Wang, Y. Y.; Gibbons, P. C.; Buhro, W. E. Lamellar Assembly of Cadmium Selenide Nanoclusters into Quantum Belts. *J. Am. Chem. Soc.* **2011**, *133*, 17005–17013.
22. Yao, W. T.; Yu, S. H.; Huang, X. Y.; Jiang, J.; Zhao, L. Q.; Pan, L.; Li, J. Nanocrystals of an Inorganic−Organic Hybrid Semiconductor: Formation of Uniform Nanobelts of ZnSe (Diethylenetriamine)0.5 in a Ternary Solution. *Adv. Mater.* **2005**, *17*, 2799–2802.
23. Chen, Y.; Vela, J.; Htoon, H.; Casson, J. L.; Werder, D. J.; Bussian, D. A.; Klimov, V. I.; Hollingsworth, J. A. "Giant" Multishell CdSe Nanocrystal Quantum Dots with Suppressed Blinking. *J. Am. Chem. Soc.* **2008**, *130*, 5026–5027.
24. Mahler, B.; Spinicelli, P.; Buil, S.; Quelin, X.; Hermier, J. P.; Dubertret, B. Towards Non-blinking Colloidal Quantum Dots. *Nat. Mater.* **2008**, *7*, 659–664.
25. Qu, L. H.; Peng, X. G. Control of Photoluminescence Properties of CdSe Nanocrystals in Growth. *J. Am. Chem. Soc.* **2002**, *124*, 2049–2055.
26. Qu, L. H.; Peng, Z. A.; Peng, X. G. Alternative Routes toward High Quality CdSe Nanocrystals. *Nano Lett.* **2001**, *1*, 333–337.
27. Yu, W. W.; Qu, L. H.; Guo, W. Z.; Peng, X. G. Experimental Determination of the Extinction Coefficient of CdTe, CdSe, and CdS Nanocrystals. *Chem. Mater.* **2003**, *15*, 2854–2860.
28. Li, J. J.; Wang, Y. A.; Guo, W. Z.; Keay, J. C.; Mishima, T. D.; Johnson, M. B.; Peng, X. G. Large-Scale Synthesis of Nearly Monodisperse CdSe/CdS Core/Shell Nanocrystals Using Air-Stable Reagents *via* Successive Ion Layer Adsorption and Reaction. *J. Am. Chem. Soc.* **2003**, *125*, 12567–12575.
29. Shiang, J. J.; Kadavanich, A. V.; Grubbs, R. K.; Alivisatos, A. P. Symmetry of Annealed Wurtzite CdSe Nanocrystals—Assignment to the C-3v Point Group. *J. Phys. Chem.* **1995**, *99*, 17417–17422.
30. Murray, C. B.; Norris, D. J.; Bawendi, M. G. Synthesis and Characterization of Nearly Monodisperse CdE (E = S, Se, Te) Semiconductor Nanocrystallites. *J. Am. Chem. Soc.* **1993**, *115*, 8706–8715.
31. Talapin, D. V.; Nelson, J. H.; Shevchenko, E. V.; Aloni, S.; Sadtler, B.; Alivisatos, A. P. Seeded Growth of Highly Luminescent CdSe/CdS Nanoheterostructures with Rod and Tetrapod Morphologies. *Nano Lett.* **2007**, *7*, 2951–2959.
32. Efros, A. L.; Rosen, M. The Electronic Structure of Semiconductor Nanocrystals. *Annu. Rev. Mater. Sci.* **2000**, *30*, 475–521.
33. Efros, A. L.; Rosen, M.; Kuno, M.; Nirmal, M.; Norris, D. J.; Bawendi, M. Band-Edge Exciton in Quantum Dots of Semiconductors with a Degenerate Valence Band: Dark and Bright Exciton States. *Phys. Rev. B* **1996**, *54*, 4843–4856.
34. Yang, C. S.; Hsieh, Y. P.; Kuo, M. C.; Tseng, P. Y.; Yeh, Z. W.; Chiu, K. C.; Shen, J. L.; Chu, A. H. M.; Chou, W. C.; Lan, W. H. Compressive Strain Induced Heavy Hole and Light Hole Splitting of $Zn_{1-x}Cd_xSe$ Epilayers Grown by Molecular Beam Epitaxy. *Mater. Chem. Phys.* **2003**, *78*, 602–607.
35. Hashimoto, J.; Nakayama, M. Lattice-Mismatch-Strain Effects on Excitons in $GaAs_{(1-x)}N_{(x)}$/GaAs Heterostructures. *Phys. Status Solidi C* **2009**, *6*, 358–361.
36. Chuang, S. L.; Chang, C. S. K·P Method for Strained Wurtzite Semiconductors. *Phys. Rev. B* **1996**, *54*, 2491–2504.
37. Bir, G. L.; Pikus, G. E. *Symmetry and Strain-Induced E□ects in Semiconductors*; John Wiley & Sons: New York, 1974.
38. Jdira, L.; Overgaag, K.; Stiufiuc, R.; Grandidier, B.; Delerue, C.; Speller, S.; Vanmaekelbergh, D. Linewidth of Resonances in Scanning Tunneling Spectroscopy. *Phys. Rev. B* **2008**, *77*, 205308.
39. Sun, Z. X.; Swart, I.; Delerue, C.; Vanmaekelbergh, D.; Liljeroth, P. Orbital and Charge-Resolved Polaron States

in CdSe Dots and Rods Probed by Scanning Tunneling Spectroscopy. *Phys. Rev. Lett.* **2009**, *102*, 196401.
40. Lakowicz, J. R. *Principles of Fluorescence Spectroscopy*, 3rd ed.; Springer: New York, 2006.
41. Landau, L.; Lifchitz, E.; Pitaevskii, L. *Electrodynamique Des Milieux Continus*, 2nd ed.; Springer: New York, 1990.
42. Chung, I. H.; Shimizu, K. T.; Bawendi, M. G. Room Temperature Measurements of the 3D Orientation of Single CdSe Quantum Dots Using Polarization Microscopy. *Proc. Natl. Acad. Sci. U.S.A.* **2003**, *100*, 405–408.
43. Muro, E.; Pons, T.; Lequeux, N.; Fragola, A.; Sanson, N.; Lenkei, Z.; Dubertret, B. Small and Stable Sulfobetaine Zwitterionic Quantum Dots for Functional Live-Cell Imaging. *J. Am. Chem. Soc.* **2010**, *132*, 4556–4557.